Chapter 26

Turbulence?

I am an old man now, and when I die and go to Heaven there are two matters on which I hope enlightenment. One is quantum electro-dynamics and the other is turbulence of fluids. About the former, I am rather optimistic.

—Sir Horace Lamb

THERE IS ONLY ONE honorable cause that would justify sweating through so much formalism - this is but the sharpening of a pencil in order that we may attack the Navier-Stokes equation,

$$\rho\left(\frac{\partial \mathbf{u}}{\partial t} + \mathbf{u}\cdot\nabla\mathbf{u}\right) = -\nabla p + \nu\nabla^2\mathbf{u} + \mathbf{f}\,, \tag{26.1}$$

and solve the problem of turbulence.

Flows described by partial differential equations [PDEs] are said to be 'infinite dimensional' because if one writes them down as a set of ordinary differential equations [ODEs], one needs infinitely many of them to represent the dynamics of one partial differential equation. Even though the state space is infinite-dimensional, the long-time dynamics of many systems of physical interest is finite-dimensional, contained within an *inertial manifold*.

Being realistic, we are not so foolhardy to immediately plunge into *the* problem – there are too many dimensions and indices. Instead, we start small, in one spatial dimension, $\mathbf{u} \to u$, $\mathbf{u}\cdot\nabla\mathbf{u} \to u\partial_x$, assume constant ρ, forget about the pressure p, and so on. This line of reasoning, as well as many other equally sensible threads of thought, such as the amplitude equations obtained via weakly nonlinear stability analysis of steady flows, leads to a small set of frequently studied nonlinear PDEs, like the one that we turn to now.

26.1 Fluttering flame front

Romeo: 'Misshapen chaos of well seeming forms!'
—W. Shakespeare, *Romeo and Julliet*, Act I, Scene I

The Kuramoto-Sivashinsky [KS] system describes the flame front flutter of gas burning on your kitchen stove, figure 26.1 (a), and many other problems of greater import, is one of the simplest nonlinear systems that exhibit 'turbulence' (in this context often referred to more modestly as 'spatiotemporally chaotic behavior'). The time evolution of the 'flame front velocity' $u = u(x,t)$ on a periodic domain $u(x,t) = u(x+L,t)$ is given by

$$u_t + \tfrac{1}{2}(u^2)_x + u_{xx} + \nu u_{xxxx} = 0\,, \qquad x \in [0,L]\,. \tag{26.2}$$

In this equation t is the time and x is the spatial coordinate. The subscripts x and t denote partial derivatives with respect to x and t: $u_t = \partial u/d\partial$, u_{xxxx} stands for the 4th spatial derivative of $u = u(x,t)$ at position x and time t. In what follows we use interchangeably the "dimensionless system size" $\tilde{L}$, or the periodic domain size $L = 2\pi\tilde{L}$, as the system parameter. We take note, as in the Navier-Stokes equation (26.1), of the "inertial" term $u\partial_x u$, the "anti-diffusive" term $\partial_x^2 u$ (with a "wrong" sign), "(hyper-)viscosity" ν, etc..

The term $(u^2)_x$ makes this a *nonlinear system*. This is one of the simplest conceivable nonlinear PDE, playing the role in the theory of spatially extended systems a bit like the role that the x^2 nonlinearity plays in the dynamics of iterated mappings. The time evolution of a typical solution of the Kuramoto-Sivashinsky system is illustrated by figure 26.1 (b). section 3.3 remark 26.1

Spatial periodicity $u(x,t) = u(x+L,t)$ makes it convenient to work in the Fourier space,

$$u(x,t) = \sum_{k=-\infty}^{+\infty} a_k(t) e^{ikx/\tilde{L}}\,, \tag{26.3}$$

with the 1-dimensional PDE (26.2) replaced by an infinite set of ODEs for the complex Fourier coefficients $a_k(t)$:

$$\dot{a}_k = \nu_k(a) = ((k/\tilde{L})^2 - (k/\tilde{L})^4)\, a_k - i\frac{k}{2\tilde{L}} \sum_{m=-\infty}^{+\infty} a_m a_{k-m}\,. \tag{26.4}$$

Since $u(x,t)$ is real, $a_k = a_{-k}^*$, and we can replace the sum in (26.4) by a sum over $k > 0$.

Due to the hyperviscous damping u_{xxxx}, long time solutions of Kuramoto-Sivashinsky equation are smooth, a_k drop off fast with k, and truncations of (26.4)

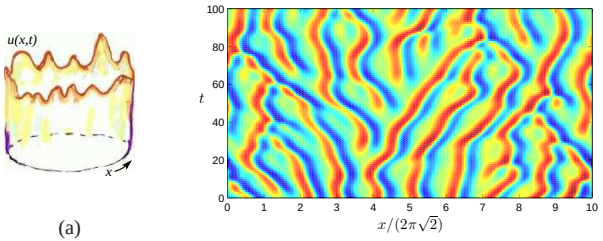

(a) (b)

Figure 26.1: (a) Kuramoto-Sivashinsky dynamics visualized as the Bunsen burner flame flutter, with $u = u(x,t)$ the "velocity of the flame front" at position x and time t. (b) A typical "turbulent" solution of the Kuramoto-Sivashinsky equation, system size $L = 88.86$. The color (gray scale) indicates the value of u at a given position and instant in time. The x coordinate is scaled with the most unstable wavelength $2\pi\sqrt{2}$, which is approximately also the mean wavelength of the turbulent flow. The dynamics is typical of a large system, in this case approximately 10 mean wavelengths wide. (from ref. [26.14])

to N terms, $16 \le N \le 128$, yield highly accurate solutions for system sizes considered here. Robustness of the Fourier representation of KS as a function of the number of modes kept in truncations of (26.4) is, however, a subtle issue. Adding an extra mode to a truncation of the system introduces a small perturbation. However, this can (and often will) throw the dynamics into a different asymptotic state. A chaotic attractor for $N = 15$ can collapse into an attractive period-3 cycle for $N = 16$, and so on. If we compute, for example, the Lyapunov exponent $\lambda(\tilde{L}, N)$ for a strange attractor of the system (26.4), there is no reason to expect $\lambda(\tilde{L}, N)$ to smoothly converge to a limit value $\lambda(\tilde{L}, \infty)$ as $N \to \infty$, because of the lack of structural stability both as a function of truncation N, and the system size $\tilde{L}$. The topology is more robust for $\tilde{L}$ windows of transient turbulence, where the system can be structurally stable, and it makes sense to compute Lyapunov exponents, escape rates, etc., for the repeller, i.e., the closure of the set of all unstable periodic orbits.

Spatial representations of PDEs (such as the $3d$ snapshots of velocity and vorticity fields in Navier-Stokes) offer little insight into detailed dynamics of low-*Re* flows. Much more illuminating are the state space representations.

The objects explored in this paper: equilibria and short periodic orbits, are robust both under mode truncations and small system parameter $\tilde{L}$ changes.

26.1.1 Scaling and symmetries

The Kuramoto-Sivashinsky equation (26.2) is space translationally invariant, time translationally invariant, and invariant under reflection $x \to -x$, $u \to -u$.

Comparing u_t and $(u^2)_x$ terms we note that u has dimensions of $[x]/[t]$, hence u is the "velocity," rather than the "height" of the flame front. Indeed, the Kuramoto-Sivashinsky equation is Galilean invariant: if $u(x,t)$ is a solution, then $v + u(x - vt, t)$, with v an arbitrary constant velocity, is also a solution. Without loss of generality, in our calculations we shall work in the mean zero velocity frame

$$\int dx\, u = 0\,. \tag{26.5}$$

In terms of the system size L, the only length scale available, the dimensions of terms in (26.2) are $[x] = L$, $[t] = L^2$, $[u] = L^{-1}$, $[\nu] = L^2$. Scaling out the "viscosity" ν

$$x \to x\nu^{\frac{1}{2}}\,, \quad t \to t\nu\,, \quad u \to u\nu^{-\frac{1}{2}}\,,$$

brings the Kuramoto-Sivashinsky equation (26.2) to a non-dimensional form

$$u_t = (u^2)_x - u_{xx} - u_{xxxx}\,, \qquad x \in [0, L\nu^{-\frac{1}{2}}] = [0, 2\pi\tilde{L}]\,. \tag{26.6}$$

In this way we trade in the "viscosity" ν and the system size L for a single dimensionless system size parameter

$$\tilde{L} = L/(2\pi\sqrt{\nu}) \tag{26.7}$$

which plays the role of a "Reynolds number" for the Kuramoto-Sivashinsky system.

In the literature sometimes L is used as the system parameter, with ν fixed to 1, and at other times ν is varied with L fixed to either 1 or 2π. Physically, varying L is the right thing to do if one is interested in taking L large, and studying 'spatio-temporal chaos.' To minimize confusion, in what follows we shall state results of all calculations in units of dimensionless system size $\tilde{L}$. Note that the time units also have to be rescaled; for example, if T_p^* is a period of a periodic solution of (26.2) with a given ν and $L = 2\pi$, then the corresponding solution of the non-dimensionalized (26.6) has period

$$T_p = T_p^*/\nu\,. \tag{26.8}$$

26.1.2 Fourier space representation

Spatial periodic boundary condition $u(x,t) = u(x + 2\pi\tilde{L}, t)$ makes it convenient to work in the Fourier space,

$$u(x,t) = \sum_{k=-\infty}^{+\infty} b_k(t) e^{ikx/\tilde{L}}\,. \tag{26.9}$$

with (26.6) replaced by an infinite tower of ODEs for the Fourier coefficients:

$$\dot{b}_k = (k/\tilde{L})^2 \left(1 - (k/\tilde{L})^2\right) b_k + i(k/\tilde{L}) \sum_{m=-\infty}^{+\infty} b_m b_{k-m} \,. \tag{26.10}$$

This is the infinite set of ordinary differential equations promised in this chapter's introduction.

Since $u(x,t)$ is real, $b_k = b^*_{-k}$, so we can replace the sum over m in (26.4) by a sum over $m > 0$. As $\dot{b_0} = 0$, b_0 is a conserved quantity, in our calculations fixed to $b_0 = 0$ by the vanishing mean $\langle u \rangle$ condition (26.5) for the front velocity.

Example 26.1 ***Kuramoto-Sivashinsky antisymmetric subspace:*** *The Fourier coefficients b_k are in general complex numbers. We can isolate the antisymmetric subspace $u(x,t) = -u(-x,t)$ by considering the case of b_k pure imaginary, $b_k = ia_k$, where $a_k = -a_{-k}$ are real, with the evolution equations*

$$\dot{a}_k = (k/\tilde{L})^2 \left(1 - (k/\tilde{L})^2\right) a_k - (k/\tilde{L}) \sum_{m=-\infty}^{+\infty} a_m a_{k-m} \,. \tag{26.11}$$

By picking this subspace we eliminate the continuous translational symmetry from our considerations; that is not an option for an experimentalist, but will do for our purposes. In the antisymmetric subspace the translational invariance of the full system reduces to the invariance under discrete translation by half a spatial period L. In the Fourier representation (26.11) this corresponds to invariance under

$$a_{2m} \to a_{2m} \,, a_{2m+1} \to -a_{2m+1} \,. \tag{26.12}$$

The antisymmetric condition amounts to imposing $u(0,t) = 0$ boundary condition.

26.2 Infinite-dimensional flows: Numerics

> The computer is not a mere mathematical excrescence, useful for technological ends. Rather, I believe that it is a meta-development that might very well change what mathematics is considered to be.
>
> — P. J. Davis [26.1]

The trivial solution $u(x,t) = 0$ is an equilibrium point of (26.2), but that is basically all we know as far as useful analytical solutions are concerned. To develop some intuition about the dynamics we turn to numerical simulations.

How are solutions such as figure 26.1 (b) computed? The salient feature of such partial differential equations is a theorem saying that for state space contracting flows, the asymptotic dynamics is describable by a *finite* set of "inertial

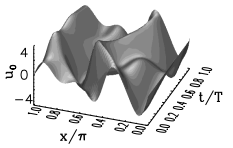

Figure 26.2: Spatiotemporally periodic solution $u_0(x,t)$, with period $T_0 = 30.0118$. The antisymmetric subspace, $u(x,t) = -u(-x,t)$, so we plot $x \in [0, L/2]$. System size $\tilde{L} = 2.89109$, $N = 16$ Fourier modes truncation. (From ref. [26.5])

manifold" ordinary differential equations. How you solve the equation (26.2) numerically is up to you. Here are some options:

Discrete mesh: You can divide the x interval into a sufficiently fine discrete grid of N points, replace space derivatives in (26.2) by approximate discrete derivatives, and integrate a finite set of first order differential equations for the discretized spatial components $u_j(t) = u(jL/N, t)$, by any integration routine you trust.

Fourier modes: You can integrate numerically the Fourier modes (26.4), truncating the ladder of equations to a finite number of modes N, i.e., set $a_k = 0$ for $k > N$. In the applied mathematics literature more sophisticated variants of such truncations are called *Gälerkin truncations*, or *Gälerkin projections*. You need to worry about "stiffness" of the equations and the stability of your integrator. For the parameter values explored in this chapter, truncations N in range 16 to 64 yields sufficient accuracy. exercise 2.6

Pseudo-spectral methods: You can mix the two methods, exploiting the speed of Fast Fourier Transforms.

Example 26.2 ***Kuramoto-Sivashinsky simulation, antisymmetric subspace:*** *To get started, we set $\nu = 0.029910$, $L = 2\pi$ in the Kuramoto-Sivashinsky equation (26.2), or, equivalently, $\nu = 1$, $L = 36.33052$ in the non-dimensionalized (26.6). Consider the antisymmetric subspace (26.11), so the non-dimensionalized system size is $\tilde{L} = L/4\pi = 2.89109$. Truncate (26.11) to $0 \le k \le 16$, and integrate an arbitrary initial condition. Let the transient behavior settle down.*

Why this $\tilde{L}$? For this system size $\tilde{L}$ the dynamics appears to be chaotic, as far as can be determined numerically. Why $N = 16$? In practice one repeats the same calculation at different truncation cutoffs N, and makes sure that the inclusion of additional modes has no effect within the desired accuracy. For this system size $N = 16$ suffices.

Once a trajectory is computed in Fourier space, we can recover and plot the corresponding spatiotemporal pattern $u(x,t)$ over the configuration space using (26.3), as in figure 26.1 (b) and figure 26.2. Such patterns give us a qualitative picture of the flow, but no detailed dynamical information; for that, tracking the evolution in a high-dimensional state space, such as the space of Fourier modes, is much more informative.

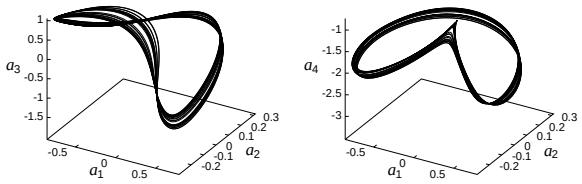

Figure 26.3: Projections of a typical 16-dimensional trajectory onto different 3-dimensional subspaces, coordinates (a) $\{a_1, a_2, a_3\}$, (b) $\{a_1, a_2, a_4\}$. System size $\tilde{L} = 2.89109$, $N = 16$ Fourier modes truncation. (From ref. [26.5].)

26.3 Visualization

> The ultimate goal, however, must be a rational theory of statistical hydrodynamics where [· · ·] properties of turbulent flow can be mathematically deduced from the fundamental equations of hydromechanics.
>
> —E. Hopf

The problem with high-dimensional representations, such as truncations of the infinite tower of equations (26.4), is that the dynamics is difficult to visualize. The best we can do without much programming is to examine the trajectory's projections onto any three axes a_i, a_j, a_k, as in figure 26.3. section 26.3

The question is: how is one to look at such a flow? It is not clear that restricting the dynamics to a Poincaré section necessarily helps - after all, a section reduces a $(d+1)$-dimensional flow to a d-dimensional map, and how much is gained by replacing a continuous flow in 16 dimensions by a set of points in 15 dimensions? The next example illustrates the utility of visualization of dynamics by means of Poincaré sections.

Example 26.3 ***Kuramoto-Sivashinsky Poincaré return maps:*** *Consider the Kuramoto-Sivashinsky equation in the N Fourier modes representation. We pick (arbitrarily) the hyperplane $a_1 = 0$ as the Poincaré section, and integrate (26.4) with $a_1 = 0$, and an arbitrary initial point $(a_2, \ldots, a_N)$. When the flow crosses the $a_1 = 0$ hyperplane in the same direction as initially, the initial point is mapped into $(a'_2, \ldots a'_N) = P(a_2, \ldots, a_N)$. This defines P, the Poincaré return map (3.1) of the $(N-1)$-dimensional $a_1 = 0$ hyperplane into itself.*

Figure 26.4 is a typical result. We have picked - again arbitrarily - a subspace such as $a_6(n+1)$ vs. $a_6(n)$ in order to visualize the dynamics. While the topology of the attractor is still obscure, one thing is clear: even though the flow state space is infinite dimensional, the attractor is finite and thin, barely thicker than a line.

The above example illustrates why a Poincaré section gives a more informative snapshot of the flow than the full flow portrait. While no fine structure is discernible in the full state space flow portraits of the Kuramoto-Sivashinsky dynamics, figure 26.3, the Poincaré return map figure 26.4 reveals the fractal structure in the asymptotic attractor.

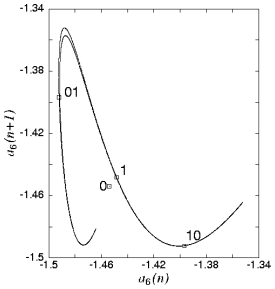

Figure 26.4: The attractor of the Kuramoto-Sivashinsky system (26.4), plotted as the a_6 component of the $a_1 = 0$ Poincaré section return map. Here 10,000 Poincaré section returns of a typical trajectory are plotted. Also indicated are the periodic points 0, 1, 01 and 10. System size $\tilde{L} = 2.89109$, $N = 16$ Fourier modes truncation. (From ref. [26.5].)

In order to find a better representation of the dynamics, we now turn to its topological invariants.

26.4 Equilibria of equilibria

(Y. Lan and P. Cvitanović)

The set of equilibria and their stable / unstable manifolds form the coarsest topological framework for organizing state space orbits.

The equilibrium condition $u_t = 0$ for the Kuramoto-Sivashinsky equation PDE (26.6) is the ODE

$$(u^2)_x - u_{xx} - u_{xxxx} = 0$$

which can be analyzed as a dynamical system in its own right. Integrating once we get

$$u^2 - u_x - u_{xxx} = c\,, \tag{26.13}$$

where c is an integration constant whose value strongly influences the nature of the solutions. Written as a 3-dimensional dynamical system with spatial coordinate x playing the role of "time," this is a volume preserving flow

$$u_x = v\,, \qquad v_x = w\,, \qquad w_x = u^2 - v - c\,, \tag{26.14}$$

with the "time" reversal symmetry,

$$x \to -x, \quad u \to -u, \quad v \to v, \quad w \to -w\,.$$

From (26.14) we see that

$$(u+w)_x = u^2 - c\,.$$

If $c<0$, $u+w$ increases without bound with $x\to\infty$, and every solution escapes to infinity. If $c=0$, the origin $(0,0,0)$ is the only bounded solution.

For $c>0$ there is much c-dependent interesting dynamics, with complicated fractal sets of bounded solutions. The sets of the solutions of the equilibrium condition (26.14) are themselves in turn organized by the equilibria of the equilibrium condition, and the connections between them. For $c>0$ the equilibrium points of (26.14) are $c_+ = (\sqrt{c},0,0)$ and $c_- = (-\sqrt{c},0,0)$. Linearization of the flow around c_+ yields Floquet multipliers $[2\lambda\,, -\lambda\pm i\theta]$ with

$$\lambda = \frac{1}{\sqrt{3}}\sinh\phi\,, \qquad \theta = \cosh\phi\,,$$

and ϕ fixed by $\sinh 3\phi = 3\sqrt{3c}$. Hence c_+ has a 1-dimensional unstable manifold and a 2-dimensional stable manifold along which solutions spiral in. By the $x\to -x$ "time reversal" symmetry, the invariant manifolds of c_- have reversed stability properties.

The non–wandering set fo this dynamical system is quite pretty, and surprisingly hard to analyze. However, we do not need to explore the fractal set of the Kuramoto-Sivashinsky equilibria for infinite size system here; for a fixed system size L with periodic boundary condition, the only surviving equilibria are those with periodicity L. They satisfy the equilibrium condition for (26.4)

$$(k/\tilde{L})^2\left(1-(k/\tilde{L})^2\right)b_k + i(k/\tilde{L})\sum_{m=-\infty}^{+\infty} b_m b_{k-m} = 0\,. \tag{26.15}$$

Periods of spatially periodic equilibria are multiples of L. Every time $\tilde{L}$ crosses an integer value $\tilde{L}=n$, n-cell states are generated through pitchfork bifurcations. In the full state space they form an invariant circle due to the translational invariance of (26.6). In the antisymmetric subspace considered here, they corresponds to two points, half-period translates of each other of the form

$$u(x,t) = -2\sum_k b_{kn}\sin(knx)\,,$$

where $b_{kn}\in\mathbb{R}$.

For any fixed period L the number of spatially periodic solutions is finite up to a spatial translation. This observation can be heuristically motivated as follows.

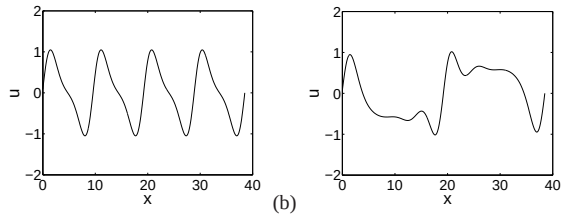

Figure 26.5: The non–wandering set under study appears to consist of three patches: the left part (S_L), the center part (S_C) and the right part (S_R), each centered around an unstable equilibrium: (a) central C_1 equilibrium, (b) side R_1 equilibrium on the interval $[0,L]$.

Finite dimensionality of the inertial manifold bounds the size of Fourier components of all solutions. On a finite-dimensional compact manifold, an analytic function can only have a finite number of zeros. So, the equilibria, i.e., the zeros of a smooth velocity field on the inertial manifold, are finitely many.

For a sufficiently small L the number of equilibria is small, mostly concentrated on the low wave number end of the Fourier spectrum. These solutions may be obtained by solving the truncated versions of (26.15).

Example 26.4 ***Some Kuramoto-Sivashinsky equilibria:***

26.5 Why does a flame front flutter?

I understood every word. section 18.2
—Fritz Haake

We start by considering the case where a_q is an equilibrium point (2.8). Expanding around the equilibrium point a_q, and using the fact that the matrix $\mathbf{A}=\mathbf{A}(a_q)$ in (4.2) is constant, we can apply the simple formula (4.25) also to the Jacobian matrix of an equilibrium point of a PDE,

$$J^t(a_q) = e^{\mathbf{A}t} \qquad \mathbf{A}=\mathbf{A}(a_q)\,.$$

Example 26.5 ***Stability matrix, antisymmetric subspace:*** *The Kuramoto-Sivashinsky flat flame front $u(x,t)=0$ is an equilibrium point of (26.2). The stability matrix (4.3) follows from (26.4)*

$$A_{kj}(a) = \frac{\partial v_k(a)}{\partial a_j} = ((k/\tilde{L})^2-(k/\tilde{L})^4)\delta_{kj} - 2(k/\tilde{L})a_{k-j}\,. \tag{26.16}$$

For the $u(x,t)=0$ equilibrium solution the stability matrix is diagonal, and – as in (4.16) – so is the Jacobian matrix $J^t_{kj}(0) = \delta_{kj}e^{((k/\tilde{L})^2-(k/\tilde{L})^4)t}$.

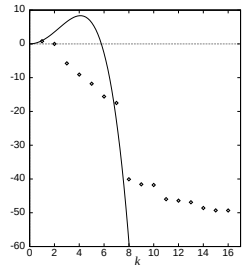

Figure 26.6: Lyapunov exponents $\lambda_{\overline{1},k}$ versus k for the least unstable spatio-temporally periodic orbit $\overline{1}$ of the Kuramoto-Sivashinsky system, compared with the Floquet exponents of the $u(x,t) = 0$ stationary solution, $\lambda_k = k^2 - \nu k^4$. The eigenvalue $\lambda_{\overline{1},k}$ for $k \geq 8$ falls below the numerical accuracy of integration and are not meaningful. The cycle $\overline{1}$ was computed using methods of chapter 13. System size $\tilde{L} = 2.89109$, $N = 16$ Fourier modes truncation. (From ref. [26.5])

For $\tilde{L} < 1$, $u(x,t) = 0$ is the globally attractive stable equilibrium. As the system size $\tilde{L}$ is increased, the "flame front" becomes increasingly unstable and turbulent, the dynamics goes through a rich sequence of bifurcations on which we shall not dwell here.

The long wavelength perturbations of the flat-front equilibrium are linearly unstable, while all short wavelength perturbations are strongly contractive. The high k eigenvalues, corresponding to rapid variations of the flame front, decay so fast that the corresponding eigen-directions are physically irrelevant. To illustrate the rapid contraction in the non-leading eigen-directions we plot in figure 26.6 the eigenvalues of the equilibrium in the unstable regime, for relatively small system size, and compare them with the Floquet multipliers of the least unstable cycle for the same system size. The equilibrium solution is very unstable, in 5 eigen-directions, the least unstable cycle only in one. Note that for $k > 7$ the rate of contraction is so strong that higher eigen-directions are numerically meaningless for either solution; even though the flow is infinite-dimensional, the attracting set must be rather thin.

While in general for $\tilde{L}$ sufficiently large one expects many coexisting attractors in the state space,in numerical studies most random initial conditions settle converge to the same chaotic attractor.

From (26.4) we see that the origin $u(x,t) = 0$ has Fourier modes as the linear stability eigenvectors. When $|k| \in (0, \tilde{L})$, the corresponding Fourier modes are unstable. The most unstable modes has $|k| = \tilde{L}/\sqrt{2}$ and defines the scale of basic building blocks of the spatiotemporal dynamics of the Kuramoto-Sivashinsky equation in large system size limit.

Consider now the case of initial a_k sufficiently small that the bilinear $a_m a_{k-m}$ terms in (26.4) can be neglected. Then we have a set of decoupled linear equations for a_k whose solutions are exponentials, at most a finite number for which $k^2 > \nu k^4$ is growing with time, and infinitely many with $\nu k^4 > k^2$ decaying in time. The growth of the unstable long wavelengths (low $|k|$) excites the short wavelengths through the $a_m a_{k-m}$ nonlinear term in (26.4). The excitations thus transferred are dissipated by the strongly damped short wavelengths, and a "chaotic equilibrium" can emerge. The very short wavelengths $|k| \gg 1/\sqrt{\nu}$ remain small for all times, but the intermediate wavelengths of order $|k| \sim 1/\sqrt{\nu}$ play an important role in maintaining the dynamical equilibrium. As the damping parameter decreases,

the solutions increasingly take on shock front character poorly represented by the Fourier basis, and many higher harmonics may need to be kept in truncations of (26.4).

Hence, while one may truncate the high modes in the expansion (26.4), care has to be exercised to ensure that no modes essential to the dynamics are chopped away.

In other words, even though our starting point (26.2) is an infinite-dimensional dynamical system, the asymptotic dynamics unfolds on a finite-dimensional attracting manifold, and so we are back on the familiar territory of sect. 2.2: the theory of a finite number of ODEs applies to this infinite-dimensional PDE as well.

We can now start to understand the remark on page 42 that for infinite dimensional systems time reversibility is not an option: evolution forward in time strongly damps the higher Fourier modes. There is no turning back: if we reverse the time, the infinity of high modes that contract strongly forward in time now explodes, instantly rendering evolution backward in time meaningless. As so much you are told about dynamics, this claim is also wrong, in a subtle way: if the initial $u(x,0)$ is *in* the non–wandering set (2.2), the trajectory is well defined both forward and backward in time. For practical purposes, this subtlety is not of much use, as any time-reversed numerical trajectory in a finite-mode truncation will explode very quickly, unless special precautions are taken.

When is an equilibrium important? There are two kinds of roles equilibria play:

"Hole" in the natural measure. The more unstable eigen-directions it has (for example, the $u = 0$ solution), the more unlikely it is that an orbit will recur in its neighborhood.

Unstable manifold of a "least unstable" equilibrium. Asymptotic dynamics spends a large fraction of time in neighborhoods of a few equilibria with only a few unstable eigen-directions.

26.6 Intrinsic parametrization

Both in the Rössler flow of example 3.3, and in the Kuramoto-Sivashinsky system of example 26.3 we have learned that the attractor is very thin, but otherwise the return maps that we found were disquieting – neither figure 3.3 nor figure 26.4 appeared to be one-to-one maps. This apparent loss of invertibility is an artifact of projection of higher-dimensional return maps onto lower-dimensional subspaces. As the choice of lower-dimensional subspace is arbitrary, the resulting snapshots of return maps look rather arbitrary, too. Other projections might look even less suggestive.

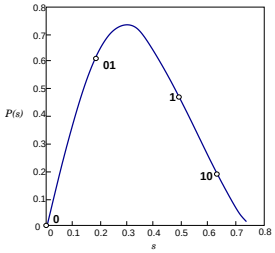

Figure 26.7: The Poincaré return map of the Kuramoto-Sivashinsky system (26.4) figure 26.4, from the unstable manifold of the $\overline{1}$ fixed point to the (neighborhood of) the unstable manifold. Also indicated are the periodic points $\overline{0}$ and $\overline{01}$.

Such observations beg a question: Does there exist a "natural," intrinsically optimal coordinate system in which we should plot of a return map?

As we shall now argue (see also sect. 13.1), the answer is yes: The intrinsic coordinates are given by the stable/unstable manifolds, and a return map should be plotted as a map from the unstable manifold back onto the immediate neighborhood of the unstable manifold.

Examination of numerical plots such as figure 26.3 suggests that a more thoughtful approach would be to find a coordinate transformation $y = h(x)$ to a "center manifold," such that in the new, curvilinear coordinates large-scale dynamics takes place in (y_1, y_2) coordinates, with exponentially small dynamics in $y_3, y_4 \cdots$. But - thinking is extra price - we do not know how to actually accomplish this.

Both in the example of the Rössler flow and of the Kuramoto-Sivashinsky system we sketched the attractors by running a long chaotic trajectory, and noted that the attractors are very thin, but otherwise the return maps that we plotted were disquieting – neither figure 3.3 nor figure 26.4 appeared to be 1-to-1 maps. In this section we show how to use such information to approximately locate cycles.

26.7 Energy budget

The space average of a function $a = a(x,t)$ on the interval L,

$$\langle a \rangle = \frac{1}{L}\int_0^L dx\, a(x,t)\,, \tag{26.17}$$

is in general time dependent. Its mean value is given by the time average

$$\overline{a} = \lim_{t\to\infty}\frac{1}{t}\int_0^t d\tau\, \langle a \rangle = \lim_{t\to\infty}\frac{1}{tL}\int_0^t\int_0^L d\tau dx\, a(x,\tau)\,. \tag{26.18}$$

The mean value $\overline{a}$, $a = a(u)$ evaluated on an equilibrium or relative equilibrium $u(x,t) = u_q(x - ct)$ is

$$a_q = \langle a \rangle_q\ . \tag{26.19}$$

Evaluation of the infinite time average (26.18) on a function of a period T_p periodic orbit or relative periodic orbit $u_p(x,t)$ requires only a single traversal of the periodic solution,

$$a_p = \frac{1}{T_p}\int_0^{T_p} d\tau\, \langle a \rangle\ . \tag{26.20}$$

Equation (26.2) can be written as

$$u_t = -V_x\,, \qquad V(x,t) = \tfrac{1}{2}u^2 + u_x + u_{xxx}\,. \tag{26.21}$$

u is related to the "flame-front height" $h(x,t)$ by $u = h_x$, so E can be interpreted as the mean energy density (26.22). So, even though KS is a phenomenological small-amplitude equation, the time-dependent quantity

$$E = \frac{1}{L}\int_0^L dx\, V(x,t) = \frac{1}{L}\int_0^L dx\, \frac{u^2}{2} \tag{26.22}$$

has a physical interpretation as the average "energy" density of the flame front. This analogy to the corresponding definition of the mean kinetic energy density for the Navier-Stokes will be useful in what follows.

The energy (26.22) is also the quadratic norm in the Fourier space,

$$E = \sum_{k=1}^{\infty} E_k\,, \qquad E_k = \tfrac{1}{2}|a_k|^2\,. \tag{26.23}$$

Take time derivative of the energy density (26.22), substitute (26.2) and integrate by parts. Total derivatives vanish by the spatial periodicity on the L domain:

$$\begin{aligned}\dot{E} &= \langle u_t\, u \rangle = -\left\langle \left(\frac{u^2}{2} + u\,u_x + u\,u_{xxx}\right)_x u \right\rangle \\ &= \left\langle +u_x\,\frac{u^2}{2} + (u_x)^2 + u_x\,u_{xxx} \right\rangle\,.\end{aligned} \tag{26.24}$$

For an equilibrium E is constant:

$$\dot{E} = \left\langle \left(\frac{u^2}{2} + u_x + u_{xxx}\right) u_x \right\rangle = E\,\langle u_x \rangle = 0\,.$$

The first term in (26.24) vanishes by integration by parts, $\left\langle (u^3)_x \right\rangle = 3\left\langle u_x\, u^2 \right\rangle = 0$, and integrating the third term by parts yet again we get that the energy variation

$$\dot{E} = \left\langle (u_x)^2 \right\rangle - \left\langle (u_{xx})^2 \right\rangle \tag{26.25}$$

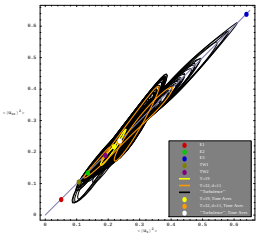

Figure 26.8: Power input $\langle (u_x)^2 \rangle$ vs. dissipation $\langle (u_{xx})^2 \rangle$ for $L = 22$ equilibria and relative equilibria, for several periodic orbits and relative periodic orbits, and for a typical 'turbulent' state. Note that $\overline{(u_{p,x})^2}$ of the $(T_p, d_p) = (32.8, 10.96)$ relative periodic orbitwhich appears well embedded within the turbulent state, is close to the turbulent expectation $\overline{(u_x)^2}$.

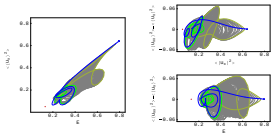

Figure 26.9: EQ_1 (red), EQ_2 (green), EQ_3 (blue), connections from EQ_1 to $A(L/4)EQ_1$ (green), from $A(L/4)EQ_1$ to EQ_1 (yellow-green) and from EQ_3 to $A(L/4)EQ_1$ (blue), along with a generic long-time "turbulent" evolution (grey) for $L = 22$. Three different projections of the $(E, \langle (u_x)^2 \rangle, \langle (u_{xx})^2 \rangle) - \langle (u_x)^2 \rangle)$ representation are shown.

balances the KS equation (26.2) power pumped in by the anti-diffusion u_{xx} against energy dissipated by the hypervicosity u_{xxxx}.

In figure 26.8 we plot the power input $\langle (u_x)^2 \rangle$ vs. dissipation $\langle (u_{xx})^2 \rangle$ for all $L = 22$ equilibria and relative equilibria determined so far, several periodic orbits and relative periodic orbits, and for a typical "turbulent" evolution. The time averaged energy density $\overline{E}$ computed on a typical orbit goes to a constant, so the expectation values (26.26) of drive and dissipation exactly balance each out:

$$\overline{\dot{E}} = \lim_{t\to\infty} \frac{1}{t} \int_0^t d\tau\, \dot{E} = \overline{(u_x)^2} - \overline{(u_{xx})^2} = 0\,. \tag{26.26}$$

In particular, the equilibria and relative equilibria sit on the diagonal in figure 26.8, and so do time averages computed on periodic orbits and relative periodic orbits:

$$\begin{aligned} \overline{E}_p &= \frac{1}{T_p} \int_0^{T_p} d\tau\, E(\tau) \\ \overline{(u_x)^2}_p &= \frac{1}{T_p} \int_0^{T_p} d\tau\, \langle (u_x)^2 \rangle = \overline{(u_{xx})^2}_p\,. \end{aligned} \tag{26.27}$$

In the Fourier basis (26.23) the conservation of energy on average takes form

$$0 = \sum_{k=1}^{+\infty} ((k/\tilde{L})^2 - (k/\tilde{L})^4)\, \overline{E_k}\,, \qquad E_k(t) = |a_k(t)|^2\,. \tag{26.28}$$

The large k convergence of this series is insensitive to the system size L; $\overline{E_k}$ have to decrease much faster than $1/(k/\tilde{L})^4$. Deviation of E_k from this bound for

small k determines the active modes. This may be useful to bound the number of equilibria, with the upper bound given by zeros of a small number of long wavelength modes.

Résumé

Turbulence is the graveyard of theories
— Hans W. Liepmann

We have learned that an instanton is an analytic solution of Yang-Mills equations of motion, but shouldn't a strongly nonlinear field theory dynamics be dominated by turbulent solutions? How are we to think about systems where every spatiotemporal solution is unstable?

Here we think of turbulence in spatially extended systems in terms of recurrent spatiotemporal patterns. Pictorially, dynamics drives a given spatially extended system through a repertoire of unstable patterns; as we watch a turbulent system evolve, every so often we catch a glimpse of a familiar pattern:

For any finite spatial resolution, the system follows approximately for a finite time a pattern belonging to a finite alphabet of admissible patterns, and the long term dynamics can be thought of as a walk through the space of such patterns. Recasting this image into mathematics is the subject of this book.

The problem one faces with high-dimensional flows is that their topology is hard to visualize, and that even with a decent starting guess for a point on a periodic orbit, methods like the Newton-Raphson method are likely to fail. Methods that start with initial guesses for a number of points along the cycle, such as the multipoint shooting method of sect. 13.3, are more robust. The relaxation (or variational) methods take this strategy to its logical extreme, and start by a guess of not a few points along a periodic orbit, but a guess of the entire orbit. As these methods are intimately related to variational principles and path integrals, we postpone their introduction to chapter 29. chapter 29

At present the theory is in practice applicable only to systems with a low intrinsic *dimension* – the minimum number of coordinates necessary to capture its essential dynamics. If the system is very turbulent (a description of its long time dynamics requires a space of very high intrinsic dimension) we are out of luck.

Commentary

Remark 26.1 Model PDE systems. The theorem on finite dimensionality of inertial manifolds of state space contracting PDE flows is proven in ref. [26.2]. The Kuramoto-Sivashinsky equation was introduced in refs. [26.3, 26.4]. Holmes, Lumley and Berkooz [26.6] offer a delightful discussion of why this system deserves study as a staging ground for studying turbulence in full-fledged Navier-Stokes equation. How good a description of a flame front this equation is not a concern here; suffice it to say that such model amplitude equations for interfacial instabilities arise in a variety of contexts - see e.g. ref. [26.7] - and this one is perhaps the simplest physically interesting spatially extended nonlinear system.

For equilibria the L-independent bound on E is given by Michelson [26.8]. The best current bound[26.9, 26.10] on the long-time limit of E as a function of the system size L scales as $E \propto L^{3/2}$.

The work described in this chapter was initiated by Putkaradze's 1996 term project (see `ChaosBook.org/extras`), and continued by Christiansen Cvitanović, Davidchack, Gibson, Halcrow, Lan, and Siminos [26.5, 26.11, 26.12, 29.16, 29.15, 26.14, 26.15, 26.13].

Exercises

26.1. **Galilean invariance of the Kuramoto-Sivashinsky equation.**

(a) Verify that the Kuramoto-Sivashinsky equation is Galilean invariant: if $u(x,t)$ is a solution, then $v + u(x + 2vt, t)$, with v an arbitrary constant velocity, i s also a solution.

(b) Verify that mean

$$\langle u \rangle = \frac{1}{L}\int_L dx\, u$$

is conserved by the flow.

(c) Argue that the choice (26.5) of the vanishing mean velocity, $\langle u \rangle = 0$ leads to no loss of generality in calculations that follow.

(d)  [thinking is extra cost] Inspection of various "turbulent" solutions of Kuramoto-Sivashinsky equation reveals subregions of "traveling waves" with locally nonzero $\langle u \rangle$. Is there a way to use Galilean invariance locally, even though we eliminated it by the $\langle u \rangle = 0$ condition?

26.2. **Infinite dimensional dynamical systems are not smooth.** Many of the operations we consider natural for finite dimensional systems do not have smooth behavior in infinite dimensional vector spaces. Consider, as an example, a concentration ϕ diffusing on $\mathbb{R}$ according to the diffusion equation

$$\partial_t \phi = \frac{1}{2}\nabla^2 \phi\,.$$

(a) Interpret the partial differential equation as an infinite dimensional dynamical system. That is, write it as $\dot{x} = F(x)$ and find the velocity field.

(b) Show by examining the norm

$$\|\phi\|^2 = \int_{\mathbb{R}} dx\, \phi^2(x)$$

that the vector field F is not continuous.

(c) Try the norm

$$\|\phi\| = \sup_{x\in\mathbb{R}} |\phi(x)|\,.$$

Is F continuous?

(d) Argue that the semi-flow nature of the problem is not the cause of our difficulties.

(e) Do you see a way of generalizing these results?

References

[26.1] P. J. Davis, "Spanning multiple worlds," *SIAM News* **41** (Dec. 2008).

[26.2] C. Foias, B. Nicolaenko, G.R. Sell, and R. Témam, "Kuramoto-Sivashinsky equation," *J. Math. Pures et Appl.* **67**, 197 (1988).

[26.3] Y. Kuramoto and T. Tsuzuki, "Persistent propagation of concentration waves in dissipative media far from thermal equilibrium," *Progr. Theor. Physics* **55**, 365 (1976).

[26.4] G.I. Sivashinsky, "Nonlinear analysis of hydrodynamical instability in laminar flames - I. Derivation of basic equations," *Acta Astr.* **4**, 1177 (1977).

[26.5] F. Christiansen, P. Cvitanović and V. Putkaradze, "Spatiotemporal chaos in terms of unstable recurrent patterns," *Nonlinearity* **10**, 55 (1997); `arXiv:chao-dyn/9606016`.

[26.6] P. Holmes, J.L. Lumley and G. Berkooz, *Turbulence, Coherent Structures, Dynamical Systems and Symmetry* (Cambridge U. Press, Cambridge 1996).

[26.7] I.G. Kevrekidis, B. Nicolaenko and J.C. Scovel, "Back in the saddle again: a computer assisted study of the Kuramoto-Sivashinsky equation," *SIAM J. Applied Math.* **50**, 760 (1990).

[26.8] D. Michelson, Steady solutions of the Kuramoto-Sivashinsky equation, Physica D **19**, 89 (1986).

[26.9] L. Giacomelli and F. Otto, New bounds for the Kuramoto-Sivashinsky equation, Comm. Pure Appl. Math. **58**, 297 (2005).

[26.10] J. C. Bronski and T. N. Gambill, Uncertainty estimates and L_2 bounds for the Kuramoto-Sivashinsky equation, Nonlinearity **19**, 2023–2039 (2006); `arXiv:math/0508481`.

[26.11] "Chaotic field theory: a sketch," *Physica* **A 288**, 61 (2000); `arXiv:nlin.CD/0001034`.

[26.12] Y. Lan, *Dynamical systems approach to 1-d spatiotemporal chaos – A cyclist's view*, Ph.D. thesis, Georgia Inst. of Tech. (2004).

[26.13] Y. Lan and P. Cvitanović, "Unstable recurrent patterns in Kuramoto-Sivashinsky dynamics," *Phys. Rev. E* **78**, 026208 (2004); `arXiv:0804.2474`.

[26.14] P. Cvitanović, R. L. Davidchack and E. Siminos, "State space geometry of a spatio-temporally chaotic Kuramoto-Sivashinsky flow," *SIAM J. Applied Dynam. Systems* (2009); `arXiv:0709.2944`.

[26.15] J. F. Gibson, J. Halcrow, and P. Cvitanović, "Visualizing the geometry of state-space in plane Couette flow," *J. Fluid Mech.* **611**, 107 (2008); `arXiv:0705.3957`.

[26.16] J. F. Gibson, *Movies of plane Couette* (Georgia Tech, 2009); `ChaosBook.orgtutorials`.

[26.17] A. K. Kassam and L. N. Trefethen, "Fourth-order time stepping for stiff PDEs," *SIAM J. Sci. Comp.*, (2004).

[26.18] Poul Martin Møller, *En dansk Students Eventyr [The Adventures of a Danish Student]* (Copenhagen 1824).

[26.19] H. K. Moffatt, Fixed points of turbulent dynamical systems and suppression of nonlinearity, Comment 1, in *Whither Turbulence! Turbulence at the Crossroads*, edited by J. L. Lumley, pp. 250–257, Springer, New York, 1990.

[26.20] J. M. Hamilton, J. Kim, and F. Waleffe, Regeneration mechanisms of near-wall turbulence structures, J. Fluid Mech. **287**, 317 (1995).

[26.21] F. Waleffe, Hydrodynamic stability and turbulence: Beyond transients to a Self-Sustaining Process, Stud. Applied Math. **95**, 319 (1995).

[26.22] F. Waleffe, On a Self-Sustaining Process in shear flows, Phys. Fluids **9**, 883 (1997).

[26.23] F. Waleffe, Three-dimensional coherent states in plane shear flows, Phys. Rev. Lett. **81**, 4140 (1998).

[26.24] F. Waleffe, Exact coherent structures in channel flow, J. Fluid Mech. **435**, 93 (2001).

[26.25] F. Waleffe, Homotopy of exact coherent structures in plane shear flows, Phys. Fluids **15**, 1517 (2003).

[26.26] R. M. Clever and F. H. Busse, Three-dimensional convection in a horizontal layer subjected to constant shear, J. Fluid Mech. **234**, 511 (1992).

[26.27] H. Faisst and B. Eckhardt, Traveling waves in pipe flow, Phys. Rev. Lett. **91**, 224502 (2003).

[26.28] H. Wedin and R. R. Kerswell, Exact coherent structures in pipe flow: Traveling wave solutions, J. Fluid Mech. **508**, 333 (2004).